Eur. Phys. J. D **7**, 341–350 (1999)

**THE EUROPEAN PHYSICAL JOURNAL D**

EDP Sciences


# A focussing funnel for metastable helium

G. Labeyrie[a], A. Browaeys, W. Rooijakkers[b], D. Voelker[c], J. Grosperrin, B. Wanner, C.I. Westbrook, and A. Aspect

Laboratoire Charles Fabry de l'Institut d'Optique, B.P. 147, 91403 Orsay Cedex, France

Received 30 October 1998 and Received in final form 27 January 1999

**Abstract.** We have constructed a magneto-optical funnel for He atoms and studied its properties using a laser cooled, highly mono-energetic atomic beam. A simple model of its action allows us to quantitatively understand the observed spot size and "focal length". We show that for a fast beam, the velocity damping coefficient plays an important role in determining the focal length of the device. The observed spot size is limited mainly by transverse heating processes which impose a transverse velocity spread. The device also permits easy scanning of the focussed spot.

**PACS.** 42.50.Vk Mechanical effects of light on atoms, molecules, electrons, and ions – 32.80.Pj Optical cooling of atoms; trapping

Metastable helium (He*) is an important atom in studies of atom optics and laser manipulation. It has already been used in demonstrations of atomic lithography [1,2] as well as other atom optics experiments [3]. There is also great interest in magneto-optical and purely magnetic trapping in order to study collision phenomena and Bose-Einstein condensation with this very simple atom. Therefore, the production of bright, intense and monochromatic beams of He* has become an important experimental problem [4].

Several characteristics of He* make its manipulation challenging: the He* is only produced in small quantities in a gas discharge (typical efficiencies are of order or below $10^{-4}$); beam velocities are very high ($> 2000$ m/s for a room temperature source); and the lifetime of the most easily accessible state is quite long (100 ns for the 2S–2P transition). The first characteristic makes it important to avoid any losses in the slowing and cooling process, while the second two mean that a cooling apparatus is necessarily quite long. An additional characteristic of helium, its small mass or alternatively, its large recoil velocity ($v_{\rm rec} = 9.2$ cm/s), also has important ramifications: while on the one hand it means that compared to, for example, Na, one requires relatively few photon absorptions to decelerate a beam by a given velocity, the transverse spreading of the beam during the slowing process is quite large. Because a cooling apparatus need be so long, transverse losses of atoms are all the more severe.

To state the problem more precisely, the rms transverse velocity $\Delta v$ acquired by the beam due to random spontaneous emissions during the slowing process is proportional to $\Delta v \propto N^{1/2} v_{\rm rec}$ where $N$ is the number of photon scattering events to slow the atoms down. If the atoms must travel some distance to an interaction region after slowing, the beam will expand by $\Delta v$ times the flight time. In addition, even if the flight time is kept very small, the beam necessarily expands spatially during slowing. The rms size of the beam $\Delta x$ after slowing is proportional to $\Delta x \propto N^{3/2} v_{\rm rec} \tau$, where $\tau$ is the atomic lifetime (see for example [5]). The relations for $\Delta v$ and $\Delta x$ demonstrate the problem of cooling helium: for a fixed temperature of the initial beam, $\Delta v$ scales roughly as $m^{-3/4}$, where $m$ is the atomic mass [5], and $\Delta x$ scales as $m^{-1/4}\tau$. Thus both the small mass and the long lifetime of the excited state pose particularly difficult problems in the case of He*.

To combat these problems we, as well as other workers [6], have used transverse cooling, both before the slowing process as well as *during* it. A convenient way to achieve the latter objective is to use a Zeeman slower whose magnetic field goes through zero partway along the deceleration path, and then to insert an atomic funnel at the zero field region. The funnel helps to refocus atoms which escape transversely from the cooled atomic beam. A funnel can also be important at the end of a Zeeman slowing region in order to concentrate atoms onto a substrate, as in typical lithography experiments or to concentrate them in the direction of a trapping region so as to increase the capture rate into a trap.

In this paper we will describe an atomic funnel that we have developed, which focuses an atomic beam of relatively fast atoms ($\sim$ 600 m/s). The length of the laser interaction region is much shorter than the distance at which the atoms converge to a spot and thus our regime

[a] e-mail: labeyrie@inln.cnrs.fr

[b] *Present address*: Sussex Centre for Optical and Atomic Physics, University of Sussex, Brighton, BN1 9QH, UK.

[c] *Present address*: Fakultät für Physik, Universität Konstanz, 78457 Konstanz, Germany.

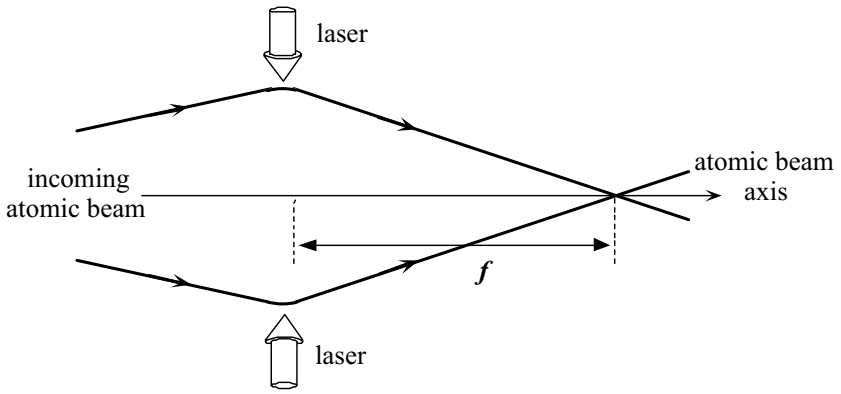


**Fig. 1.** The focussing funnel. An atomic beam interacts for a short time with the funnel laser beams in a magnetic field gradient (not represented). When leaving the interaction region, the atoms' transverse velocities are directed towards the beam axis; after a free flight all trajectories cross the axis at the same point, at a distance $f$ from the laser interaction region (the "focal length" of the funnel). In this picture, the transverse and longitudinal dimensions are not drawn to scale.

of operation is quite different from that of most previous funnels. A schematic diagram is shown in Figure 1. We begin with a qualitative description in which we discuss a sort of "thin lens" regime in which we may assume that the transverse atomic velocity is deviated while leaving the atoms' transverse position unchanged. Then we will give a simple theoretical description of the funnel based on a damped harmonic oscillator model. This model is simple enough to permit the derivation of analytical formulae for important characteristics as the size and location of the focal spot. We will then discuss experiments we have performed which quantitatively test the model. We find in particular a much improved agreement between the measurements and the model if we take into account the velocity lag associated with the damping.

## 1 Qualitative description of the funnel

An atomic funnel transversely concentrates an atomic beam using the principle of the magneto-optical trap [7] in the two dimensions transverse to the atomic beam. The atoms are subject to both a friction force which damps their transverse velocities and to a linear restoring force pushing them towards the axis defined by the funnel. In most atomic funnels described to date [8–10], the interaction time was sufficiently long to compress the position distribution of the atoms into a very narrow, highly collimated beam of atoms. More precisely, the interaction time is much longer than the damping time of both the transverse position and velocity in the funnel. This long interaction time is possible because fairly slow (10–100 m/s) atoms were used as inputs to the funnels.

In attempting to insert a funnel partway along the Zeeman cooling path of a He* beam, long interaction times are quite difficult to achieve because the atoms are still moving quite fast. One can, however, still exploit the remarkable properties of the magneto-optical force by noting that velocity damping times are typically much shorter than position damping times. In other words, motion in a magneto-optical trap is typically strongly overdamped. Thus it is possible to damp the transverse velocity even of a fast beam of atoms (the typical time scale of the velocity damping is $\hbar$ divided by the recoil energy). The transverse atomic velocity damps quickly to a value such that the Zeeman shift at the position of the atom is equal to the Doppler shift. Thereafter, the velocity is "locked" to the slowly evolving position. After a few velocity damping times the atoms are all moving towards the axis with velocities proportional to their transverse position. The atoms leave the funnel and all cross the axis defining the funnel at the same time. If the longitudinal velocity distribution is narrow they will also all cross the axis at nearly the same point in space. Thus a funnel with a short interaction time acts as a sort of dissipative lens, characterized by a velocity dependent focal length, taking an arbitrary transverse phase space at the input to a beam converging to a single point. We will refer to this type of device as a "focussing funnel".

The focussing funnel was discussed and demonstrated on an uncooled beam of Ne* atoms in reference [6]. A "focal spot" of a few mm was observed and the authors attributed this size to chromatic aberration of the device, *i.e.* the fact that the focal length of the funnel is velocity dependent. We have constructed a similar device in our laboratory. In contrast to reference [6], our funnel was at the end of a Zeeman cooling apparatus and so we were able to study the funnel with a highly monochromatic beam of atoms. We find spot sizes quite similar to those observed in reference [6] in spite of our longitudinal cooling, and a simple model of our funnel indicates that the size of the spot is actually limited by the dispersion in transverse velocities.

As in reference [6], we use an increasing magnetic field gradient in the interaction region. We do this because the spatial and velocity capture range of the funnel is larger for smaller gradients, while the focal length is mostly determined by the magnetic field gradient at the end of the interaction. Thus we are able to maximize the capture range while minimizing the focal length of the funnel. We have found an effect due to the finite value of the velocity damping coefficient that modifies the simple formula: "Zeeman shift equals Doppler shift" inside the funnel. This happens when the field gradient increases so rapidly that the atomic velocity lags somewhat the steady state value at a given transverse position. This effect lengthens the effective focal length of the funnel observed in the experiment.

## 2 Damped harmonic oscillator model

We will use a damped harmonic oscillator model to describe the action of the funnel, deriving approximate analytical expressions for the focal length and the spot size. We simply assume that the atoms feel a friction force linear in velocity and characterized by a coefficient $\alpha$. The quantity $\alpha$ in our experimental situation will be estimated using a Doppler cooling model (see Sect. 5). We will also assume that the restoring force in the MOT is found by introducing a spring constant $K$, given by [11]:

$$K = \alpha \frac{\mu}{\hbar k} b.$$

Here $\mu$ describes how the atomic resonance frequency varies as a function of magnetic field. In the case of He*, the relevant Zeeman sublevels are $J = 1$, $m_{\rm J} = 1$, in the ground state and $J = 2$, $m_{\rm J} = 2$ in the excited state, which gives $\mu/\hbar = \mu_{\rm B}/\hbar = 1.4$ MHz/G. The quantity $b$ is the gradient of the $x$ (transverse) component of the magnetic field, $\partial B_x/\partial x$. We wish to model a situation in which $b$ is a function of $z$, the longitudinal position of the atom in the funnel. We will model this increase by writing $b(z) = b_0 G(z)$ where $b_0$ is the field gradient at the beginning of the interaction region and $z$ is the position of the atom measured from the beginning of the interaction region. The function $G(z)$ is therefore dimensionless and $G(0) = 1$.

If we imagine the motion of the atoms of mass $m$ in a reference frame moving along $z$ with the atoms, and we neglect the fluctuating part of the force due to the quantized nature of momentum exchange between the atoms and the laser field, their transverse motion is described by the following differential equation:

$$\ddot{x} + \gamma\, \dot{x} + \omega^2 F(t) x = 0 \tag{1}$$

with $F(t) = G(v_z t)$, $\gamma = \alpha/m$ and $\omega^2 = K(b_0)/m$. This is an equation for a simple harmonic oscillator with a time dependent spring constant. Including a fluctuating force and then averaging the equation over a time scale long compared to the fluctuations yields the same differential equation for the mean values of $x, \dot{x}$ and $\ddot{x}$. Note also that for our parameters the oscillator is overdamped *i.e.* $\omega < \gamma/2$, and thus the lens is purely dissipative.

Now we will use this model to estimate two important features of the funnel, the focal distance, at which the beam converges, and the size of the beam at that point.

*The focal length of the funnel.* Since the interaction length is short, the focal length $f$ of the funnel is given by the relation between the transverse velocity and the transverse position of the atoms at the output of the funnel ($f = x/\dot{x}|_{\rm out} v_z$). The simplest way to estimate $f$ is to suppose that the large value of the damping coefficient allows one to neglect $\ddot{x}$ compared to the other terms in equation (1). This gives:

$$\gamma\, \dot{x}\,(t_{\rm int}) = -\omega^2 F(t_{\rm int}) x\,(t_{\rm int})\,, \tag{2}$$

were $t_{\rm int}$ is the interaction time. This corresponds to assuming that the velocity is always "locked" to the local position, or that the Doppler shift compensates the Zeeman shift inside the funnel, as was done in reference [6]. In this case the longitudinal velocity and the magnetic field gradient at the output of the funnel are the only parameters determining the focal length, and one finds

$$f = v_z \frac{\hbar k}{\mu_{\rm B} b_{\rm f}} \tag{3}$$

were $b_{\rm f}$ is the field gradient at the end of the interaction region.

A different approximation is possible, however, if one uses the fact that the interaction time is much shorter than the damping time of the position $((\omega^2/\gamma)F(t))^{-1}$ (the "thin lens" approximation). In this case, the atom's position hardly changes during the interaction and one can replace $x$ in the differential equation by a constant $x_0$, the position of the atom when entering the funnel. In this case one has an expression for $\dot{x}$ as a function of $x_0$ and $t_{\rm int}$ the interaction time:

$$\dot{x} = x_0 \omega^2 {\rm e}^{-\gamma t_{\rm int}} \int_0^{t_{\rm int}} {\rm e}^{\gamma t} F(t) {\rm d}t + \dot{x}\,(0) {\rm e}^{-\gamma t_{\rm int}}. \tag{4}$$

The second term may be dropped if the interaction time is long compared to the velocity damping time, as we will assume in the following.

It is useful to discuss the simple special case of a linearly increasing gradient, $F(t) = (1 + \beta t)$. In this case we have (again assuming $\gamma t_{\rm int} \gg 1$):

$$\dot{x}\,|_{\rm out} = x_0 \frac{\omega^2}{\gamma} \left(1 + \beta t_{\rm int} - \frac{\beta}{\gamma}\right) \tag{5}$$

yielding the same expression as in equation (2) except for the correction due to term $\beta/\gamma$. This is the "lag" discussed at the end of Section 1, leading to a somewhat lower velocity for a given transverse position, and a slightly longer focal length than in the estimate of equation (3):

$$f = v_z \frac{\hbar k}{\mu_{\rm B} b_{\rm f}} \left(1 - \frac{\beta}{\gamma(1 + \beta t_{\rm int})}\right)^{-1}. \tag{6}$$

Typically, in our experiment $\beta t_{\rm int} \gg 1$ so that the fractional correction to the focal length is approximately $1/\gamma t_{\rm int}$.

To get a feel for the quality of this approximation, we can compare a numerical solution of equation (1) and the approximate ones under our typical experimental conditions. In Figure 2 we show the evolution of the transverse velocity as a function of time according to the three models. The parameters are: $\omega \approx 3 \times 10^3$ s$^{-1}$, $\gamma \approx 6 \times 10^4$ s$^{-1}$, $\beta \approx 9 \times 10^4$ s$^{-1}$, and $t_{\rm int} = 10^{-4}$ s, corresponding to a gradient which increases linearly from 1 G/cm to 10 G/cm in 100 $\mu$s. The other parameters are also typical for our experiment. The two straight lines correspond to the equations (3, 6). The curved lines correspond to the numerical solution for an initial position $x_0 = 5$ mm, and two different initial transverse velocities. One sees that first, the lag term represents a substantial correction to the velocity, and second, that the exact solutions approach

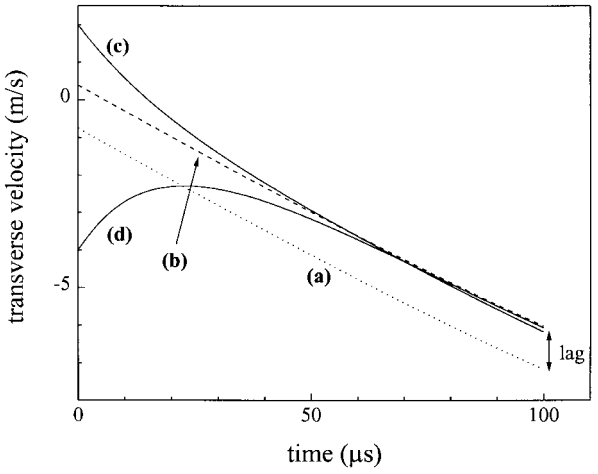


**Fig. 2.** Evolution of the transverse velocity in the funnel. The parameters are $\omega \approx 3\times10^3$ s$^{-1}$, $\gamma \approx 6\times10^4$ s$^{-1}$ ($\approx (17\ \mu\text{s})^{-1}$), $\beta \approx 9\times10^4$ s$^{-1}$ and $x_0 = 5$ mm. Curves (a) and (b) correspond to the approximate solutions without (Eq. (2)) and with the lag term (Eq. (5)), respectively. Curves (c) and (d) show the numerical solutions of equation (1), for two values of the initial velocity.

very closely the approximate solution including the effects of lag.

*Size of the focal spot.* The most important contributions to the size of the focussed beam are: (1) the spread in longitudinal velocities and (2) the spread in transverse velocities. These two contributions can be estimated by simply assuming that $f = x/\dot{x}|_{\text{out}} v_z$ and using our knowledge of the longitudinal and transverse velocity spreads. The rest of the damped harmonic oscillator model is not necessary.

(1) Size due to the longitudinal velocity spread $\Delta v_z$, or the chromatic aberration of the funnel: the size of the focal spot $\Delta x$ in the $x$ direction is $\Delta x = (\Delta v_z/v_z)x_0$, where $x_0$ is the transverse position of the atom at the exit from the laser interaction region. Our measurements of the longitudinal velocity spread after cooling (see below), indicate $(\Delta v_z/v_z) < 0.01$, while the maximum exit radius is less than 2 cm. Thus the contribution due to the longitudinal velocity spread should be smaller than 0.2 mm.

(2) Size due to the transverse velocity spread $\Delta v_x$: although the action of the funnel causes the transverse velocity to lock to a value determined by the transverse position $x_0$, there is, as always in laser cooling, a spread of velocities about this value due to fluctuations in the average radiation pressure force exerted by the lasers. The position spread due to this effect is simply the product of $\Delta v_x$ and the time of flight between the funnel exit and the focal point. If we neglect the lag this gives: $\Delta x = \Delta v_x \gamma/\omega^2$. To estimate $\Delta v_x$ we note that the Doppler cooling limit for He* in 3D is $\Delta v_x = 0.3$ m/s. However our laser linewidth is larger than the natural linewidth of the transition, and the beam intensity is very high (see Sect. 3) therefore we certainly expect $\Delta v_x$ to be larger than this limit. This expectation is confirmed by measurements by several groups which find typical velocity spreads in 3D MOTs of order 1 m/s for He [12–14]. If we assume a velocity spread, $\Delta v_x = 1$ m/s, we find $\Delta x = 1$ mm, very close to our observations. Therefore it appears to us that this is the limiting factor in the size of our focussed spot.

It is interesting to note that this size is different from the steady state size of a 3D MOT if we assume that a MOT is described by a damped harmonic oscillator equation. For a MOT, $\Delta x = \Delta v_x/\omega$, which is smaller by a factor of $\omega/\gamma$. In the case of our funnel, and using the exit value of the field gradient to calculate $\omega$, we find that this factor is of order 0.1–0.5. The larger the field gradient, the smaller should be the focal spot.

In principle the funnel may also have "spherical aberrations" due to the nonlinearity of the friction force as a function of velocity and due to nonlinearity of the magnetic field gradient. Comparisons between the linearized friction model and numerical integration of trajectories including the full velocity-dependence of the friction force indicate that departures from linear friction are negligible for typical parameters in our experiment. Our measurements of the field profiles in the transverse direction also indicate that contributions of nonlinear transverse magnetic field gradients are negligible.

## 3 Description of experiment

Experiments were carried out using a beam of metastable helium, He*, in the $2^3S_1$ state. The beam design is similar to that of reference [4]. More details of our source can be found in reference [15]. Briefly, the metastable atoms were produced in a DC discharge using a skimmer as the anode, and a brass needle as the cathode. The discharge was cooled by liquid nitrogen. Measurements of fluorescence using the Doppler effect indicated a velocity distribution centered at 1300 m/s with a FWHM of 300–400 m/s. The measured intensity was of order $10^{14}$ s$^{-1}$sr$^{-1}$.

The metastable beam was transversely laser cooled by a two dimensional molasses using a diode laser tuned to the $2^3S_1$–$2^3P_2$ transition ($\lambda = 1.083$ $\mu$m). The molasses interaction region was located 4 cm behind the skimmer and had a length of 10 cm. This cooling increased the on axis intensity of the metastable beam, measured at a distance of 3.3 m behind the skimmer, by about a factor of 10–20.

After transverse collimation the beam enters a tapered solenoid (the Zeeman slower). The longitudinal magnetic field in this region increases rapidly to a maximum of $B_0 = 420$ G and then slowly diminishes to zero following roughly a profile $B = B_0\sqrt{1 - z/a}$ were $a \approx 1.9$ m. The solenoid consists of 20 layers of copper windings of different lengths. A circularly polarized laser beam tuned to the red of the $2^3S_1$–$2^3P_2$ transition longitudinally slows and cools the beam. The slowing laser power was 30 mW. Its diameter was 3 cm at the output of the Zeeman slower and it was approximately focussed onto the skimmer. With this setup we were able to slow the atomic beam to a selectable velocity between 300 and 900 m/s. When slowing to 500 m/s, we are able to slow about 1/3 of the available

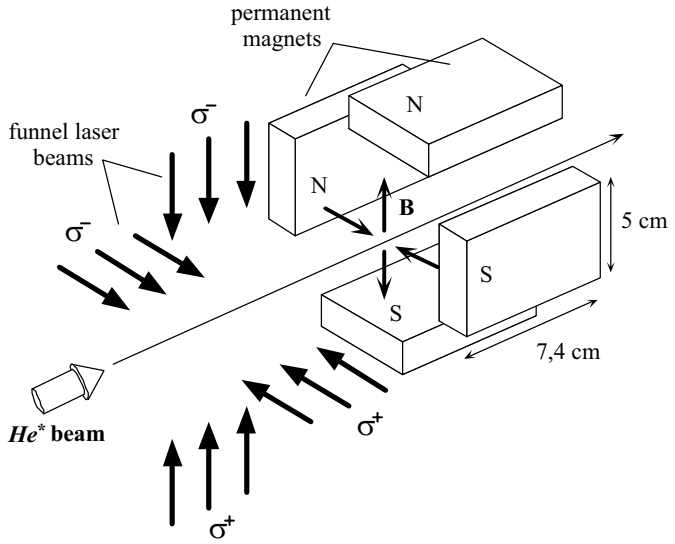


**Fig. 3.** Schematic view of the funnel. After exiting the Zeeman slower, the atomic beam enters the interaction region with the funnel laser beams of length five centimeters. During this interaction, the atoms experience an increasing magnetic field gradient created by four permanent magnets in a linear quadrupole configuration.

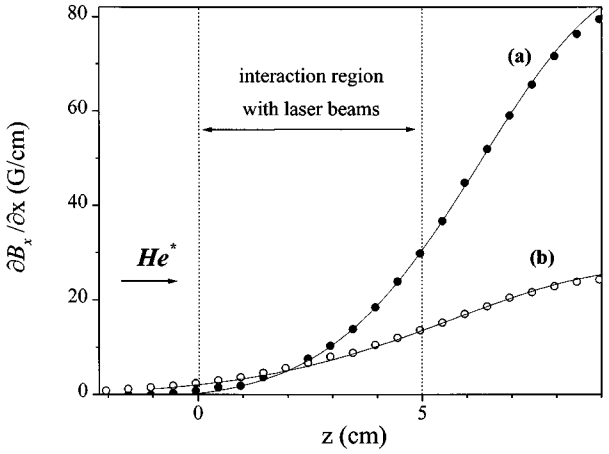


**Fig. 4.** Measurements of the magnetic field gradient profile along the beam axis. Curves (a) and (b) correspond to a distance between the magnets and the axis of 6.5 cm and 9.7 cm respectively. The solid lines show the calculated profiles. The vertical lines show the region where the funnel laser beams are applied.

atoms. Measurements of the Doppler profile of the slowed beam allow us to place an upper limit of $\Delta v_z < 5$ m/s on the longitudinal velocity spread.

The funnel is placed at the output of the Zeeman slower. The atoms drift for 10 cm and then enter the laser interaction region whose length is 5 cm. The intensity of the funnel laser beams corresponded to 10 mW per beam over a waist of approximately $5 \times 2$ cm$^2$. The laser frequency was locked to the atomic transition in a saturated absorption cell. A small detuning was introduced by slightly tilting each laser beam with respect to the plane orthogonal to the atomic beam axis, by an angle $\theta$ (the laser beams are then no longer parallel). The effective (red) detuning is then $\theta v_z/\lambda$, which gives about 0.5 MHz for $\theta = 1$ mrad and $v_z = 500$ m/s. In a typical experiment, the angle $\theta$ was optimized to give the smallest atomic spot. Immediately after the laser interaction region there are 4 permanent ferrite magnets placed in a linear quadrupole configuration (see Fig. 3). This configuration of the magnets creates a field gradient $b = \partial B_x/\partial x$ which increases as the atoms pass through the laser beams. The magnets are $7.4 \times 5 \times 2$ cm$^3$ and are placed 6 to 12 cm from the axis of the atomic beam. The magnetic field at the surface of each magnet was measured to be 850 G. Measurements of $b$ as a function of $z$ are shown in Figure 4. In the absence of the laser beams the effect of the magnetic field on the atoms' trajectories is negligible.

## 4 Measurement techniques

We performed a series of measurements of the size of the atomic beam for various configurations of the Zeeman slower and the funnel. Note that it is necessary to make these measurements *without interrupting* the slowing laser. Thus an optical detection scheme is desirable. To this end we developed the scannable laser absorption detection system shown in Figure 5. We use a galvo-driven rotating mirror to vary the angle of incidence of a collimated laser beam (intensity 2 mW) on a cylindrical lens of focal length 20 cm. The mirror is at the focus of the lens and therefore after the lens the beam executes a translation parallel to the axis of the optical system. In addition, the lens focuses the beam to a waist of 260 $\mu$m $\times$ 1.5 cm for good spatial resolution. The laser beam exits at the opposite side of the vacuum system and a second lens collects the transmitted light and focuses it onto a photodiode. The laser is frequency modulated (by modulation of the injection current) at 15 kHz, the frequency excursion is about 2 MHz. The photodiode signal is demodulated at that frequency by a lock-in amplifier with a typical time constant of 1–3 ms. The atomic absorption signal has the advantage of being insensitive to the scattered light in the vacuum chamber, and in addition one obtains immediately a measurement of the optical thickness of the atomic beam.

The system could be tilted out of the plane of Figure 5 so as to be sensitive to the longitudinal velocity. The ability to detect a specific longitudinal velocity class is important since in many cases our atomic beam contains an irrelevant, uncooled component. Typical tilt angles were of order 5 degrees out of the plane of Figure 5 (or 85 degrees to the atomic beam axis). To make a transverse beam profile measurement, we locked the laser frequency at a point where the lock-in signal was maximal (*i.e.* where the derivative of the absorption signal was maximum) and then scanned the detection beam slowly (in about 1 s) across the transverse profile of the slowed atomic beam. These scans could be repeated and averaged, if necessary, on a digital oscilloscope. This system permitted real time optimization of the funnel parameters.

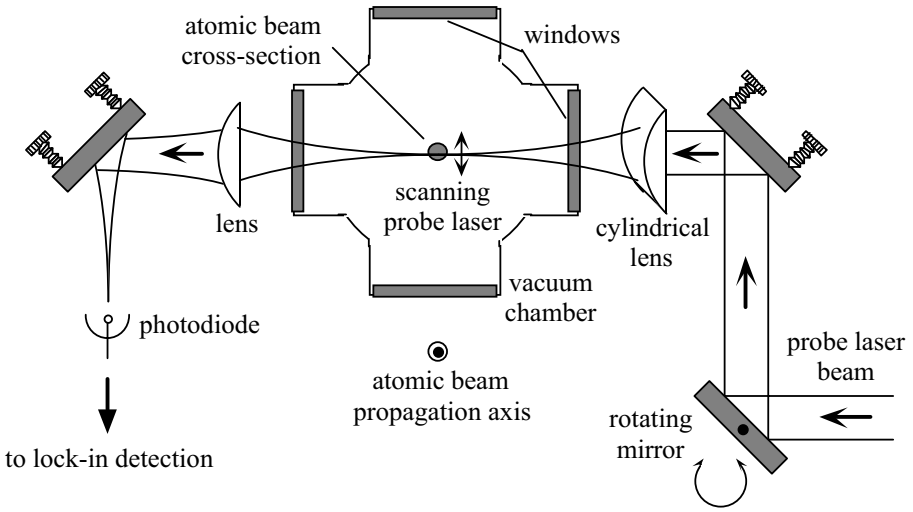


**Fig. 5.** The scanning probe detection technique. A frequency-modulated probe laser beam is focussed on the atomic beam with a cylindrical lens. A galvo-driven rotating mirror, placed at the focal point of the lens, allows a vertical scan of the probe across the atomic beam section. The transmitted light is detected using a lock-in scheme.

This technique only gives information on the atom distribution along the direction of translation of the detection beam. To get two dimensional information, we use a thin sheet of light intersecting the atomic beam. This light sheet consisted of a laser beam 4 cm × 1 mm, which was tilted at 45° with respect to the atomic beam propagation axis. A cooled CCD camera recorded the fluorescence of the atoms as they passed through the probe. As in the scanning beam technique, we rendered the fluorescence velocity selective by choosing the propagation direction of the light sheet to be at a slight angle to the plane orthogonal to the atomic beam axis. A several minute exposure followed by a background substraction permitted observation of the focussed beam cross-section with good signal to noise.

The velocity sensitivity of our detection also has a disadvantage. If we use the funnel to strongly focus the atoms in two dimensions, the resulting beam has a large velocity spread in the direction of propagation of the detection beam. The signals of the scanning probe as well as the sheet of light will thus be diminished. In the case of the spatially scanning probe beam we chose to concentrate on measuring the characteristics of the funnel when operating in 1D, that is with only one pair of counterpropagating laser beams acting on the atoms in the presence of a linear quadrupole field. In the case of the sheet of light/fluorescence detection, we scanned the frequency of the laser beam across the Doppler width of the focussed beam during exposure, to record the signal from all transverse velocities.

## 5 Experimental results

Before using the funnel we performed measurements of the transverse size of the atomic beam as a function of the final velocity after the Zeeman slower. The detection beam was placed about 70 cm after the focussing funnel. The results are shown in Figure 6, and clearly show the effect of the transverse spreading. Simple models of the expected beam size along the lines of reference [5] predict a

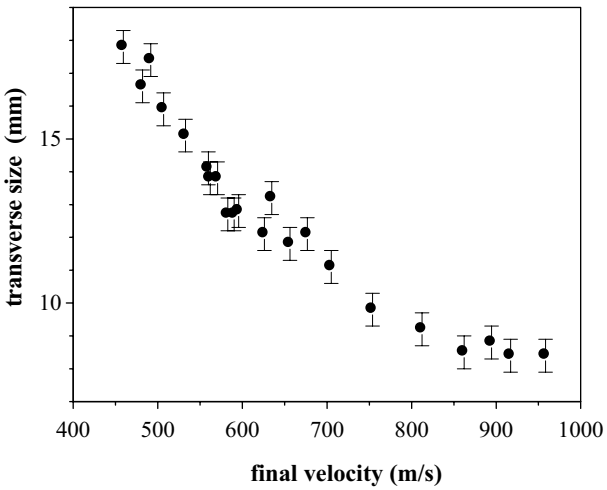


**Fig. 6.** Observation of the transverse spreading. The transverse size of the atomic beam (FWHM) is measured 70 cm after the Zeeman magnet, as a function of its final velocity. As expected, one observes that the beam spreads as it is further slowed down. The beam diameter is about 1.5 cm for a final velocity of 500 $ms^{-1}$.

larger beam size for low final velocities than we observed. The difference is about a factor of 2 for a final velocity of 500 m/s. We are not sure why this is so but the discrepancy may have to do with aperturing of the atomic beam in the beam tube. Even so it is clear that our beam has expanded a great deal in slowing from 1200 m/s to 500 m/s illustrating the importance of a funnel for He*.

To demonstrate the effect of the funnel we show in Figure 7a comparison of two scans at the same position without a funnel and with a 1D funnel. We observe that the funnel takes nearly all the atoms from the initial 15 mm wide distribution into a peak of width 1.8 mm. A similar experiment can be done with a 2D funnel, using the sheet of light probe as a detector. A typical result is shown in Figure 8. A comparable focal spot size is observed. The increase in atomic intensity in 2D is about a factor of 20.

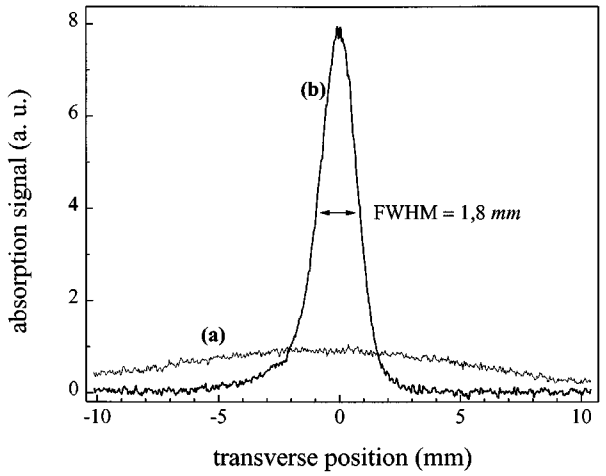


**Fig. 7.** Effect of the 1D funnel, recorded with the scanning probe technique. Curves (a) and (b) are two transverse profiles of the atomic beam obtained without and with the funnel laser beams on, respectively. The measurement is performed 46 cm after the exit of the funnel, for a 500 $\mathrm{ms}^{-1}$ atomic beam. The initial distribution (a) is about 1.5 cm wide; the funnel concentrates nearly all the atoms into a spot of diameter 1.8 mm. These profiles were averaged over ten scans (integration time $\sim 10$ s).

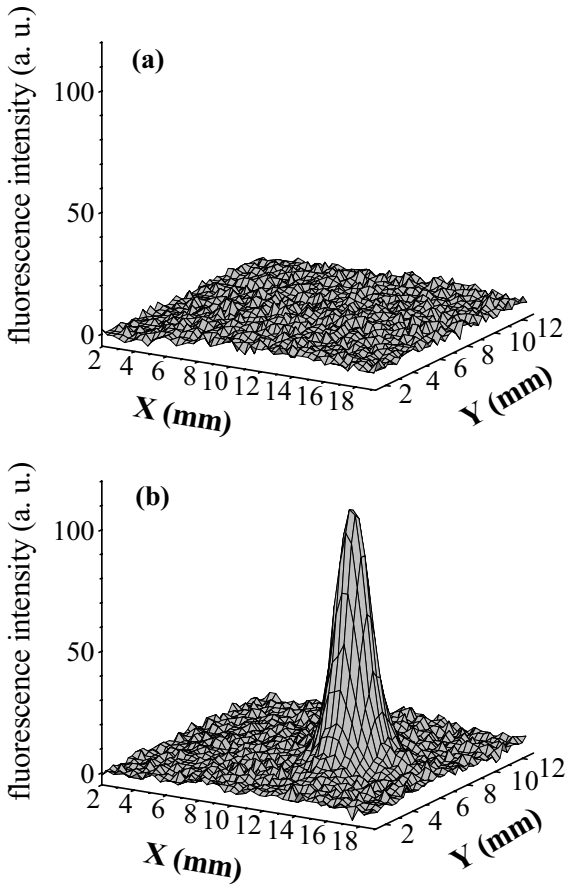


**Fig. 8.** Effect of the 2D funnel. This figure shows plots of the fluorescence intensity distribution recorded when the atomic beam crosses a sheet of light: (a) funnel off, (b) funnel on. The exposure time is 5 minutes. The focussed beam size is about 2 mm FWHM; the atomic density is increased by a factor 20.

Using the 1D configuration we then made a study of the "waist" $\Delta x$ of the focussed atomic beam as a function of position $z$ along the axis. This was done by keeping the funnel parameters fixed and placing the scanning beam detector at various positions. The results are shown in Figure 9. One clearly sees the convergence and then re-expansion of the atomic beam. An arrow has been added to show the position where one expects to find the focus if one assumes that the transverse velocity at the output of the funnel is simply given by $f = v_z \hbar k / \mu b_\mathrm{f}$ *i.e.* if one neglects the effect of the lag. In the situation depicted in Figure 9 the lag effect is clearly very important.

To analyze the lag in detail we would like to perform measurements such as that in Figure 9 for many different combinations of the parameters of the funnel. Doing the experiment exactly as was done to obtain Figure 9 is rather difficult since it requires moving the detector, and often modifying the vacuum system for each data point. Instead we can obtain similar information by keeping the detection position $z$ fixed and varying either the longitudinal velocity of the atomic beam $v_z$ (by changing the current in the Zeeman cooler and the detuning of the slowing laser) or the magnetic field gradient (by moving the permanent magnets) in such a way as to scan the focal spot through the detector. The two examples shown in Figures 10 and 11, show that such scanning of the focus is easily visualized. Again the significance of the lag is emphasized by the arrows which show the expected minimum if one ignores the lag.

We used a crude model to fit the experimental data (solid lines in Figs. 10 and 11). The atomic beam diameter $w$ measured at position $z$ is assumed to follow the expression

$$w = \Delta x \sqrt{1 + \left(x_0^2/\Delta x^2 - 1\right)\left(1 - z/f\right)^2},$$

where $\Delta x$ and $x_0$ are the beam sizes at the focus and the funnel output respectively. The atomic waist $\Delta x$ is directly measured in the experiment while the parameter $x_0$ is adjusted; the focal length $f$ is computed using equation (6), in which the only adjustable parameter is the damping coefficient $\gamma$. The value of $\gamma$ consistent with the data of Figures 10 and 11 is about $(30\ \mu\mathrm{s})^{-1}$. We emphasize that this fit is a crude approximation, since we expect both $\Delta x$ and $x_0$ (and even $\gamma$, as will be discussed at the end of this section) to vary when the beam velocity and field gradient are modified (for instance, the atomic waist $\Delta x$ should vary with the beam velocity $v_z$, see Sect. 2). But again, it is clear that taking into account the lag term dramatically improves the agreement with experiment.

We summarize in Figure 12 the results of several scans as in Figure 10 in which the funnel parameters (laser intensity and tilt angle $\theta$) and the detector position were fixed, and $v_z$ was varied to bring the beam to a focus at the detector position (46 cm downstream the funnel

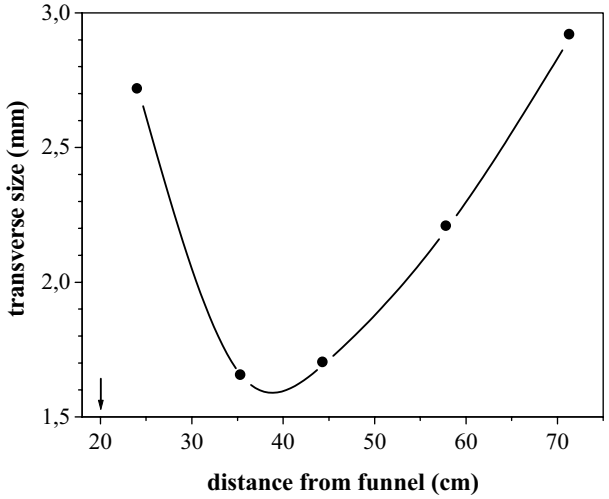


**Fig. 9.** Demonstration of the focussing. The transverse size of the atomic beam is measured as a function of the distance from the exit of the funnel. One clearly observes the contraction followed by the re-expansion of the beam. The atomic "waist", of size approximately 1.6 mm, is located at about 40 cm from the funnel. The arrow points out the expected focal length if the lag effect is neglected. The solid line was added to guide the eye and does not correspond to a fit.

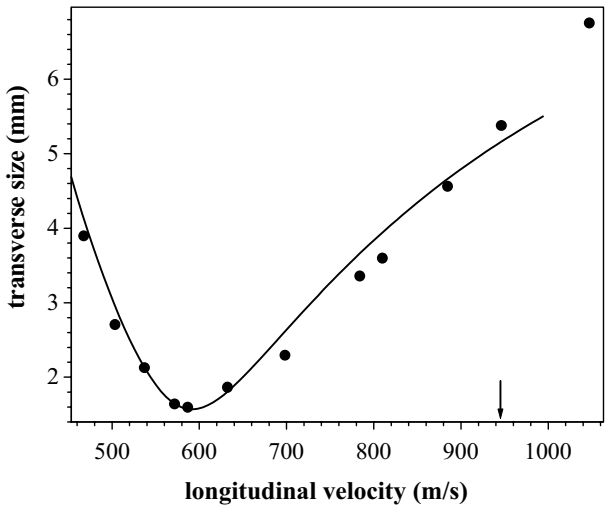


**Fig. 10.** Effect of longitudinal velocity on focus position. The transverse size of the atomic beam is measured at a fixed distance from the funnel ($z$ = 46 cm), as a function of its velocity. The magnetic field gradient at the output of the funnel is 13.5 Gcm$^{-1}$. As in Figure 9, the arrow corresponds to the expected waist position if the lag is neglected. The solid line corresponds to the fit discussed in the text.

output) for various values of field gradient $b_{\rm f}$. To compare these results to the simple harmonic oscillator model, we use equation (4) with $t_{\rm int} = l/v_z$, were $l$ is the length of the interaction region (5 cm). We stress that, for our parameters, the solutions of equation (4) are almost indistinguishable from those of equation (1) as was shown in Figure 2. The straight line (a) in Figure 12 is the prediction assuming no lag effect (*i.e.* a very large value of $\gamma$).

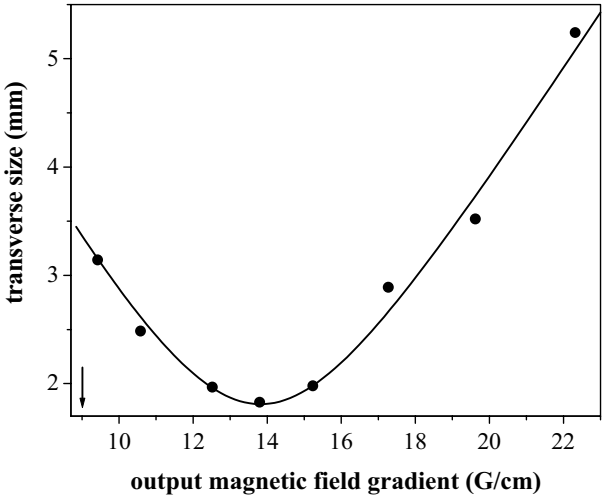


**Fig. 11.** Effect of magnetic field gradient on focus position. The transverse size of the atomic beam is measured as a function of the magnetic field gradient at the output of the funnel, at a fixed distance from the funnel (46 cm) and for a velocity of 630 ms$^{-1}$. The arrow points the expected waist position if the lag is neglected. The solid line is obtained using the same fitting procedure as in Figure 10, yielding $\gamma = (28\ \mu{\rm s})^{-1}$.

To evaluate the effect of the lag it is necessary to know independently the value of the friction coefficient and the variation of the field gradient in the interaction region (the function $F(t)$).

To get an idea of the value of the friction coefficient one can use the 1D, two level model described in reference [16]. In that model the friction coefficient is given by:

$$\alpha = 4\hbar k^2 I/I_0 \frac{\dfrac{2\Delta}{\Gamma}}{\left[1 + 2I/I_0 + \left(\dfrac{2\Delta}{\Gamma}\right)^2\right]^2}\cdot \qquad (7)$$

This expression is quite accurate, even for high intensities in a $J_{\rm g} = 0 \leftrightarrow J_{\rm e} = 1$ transition illuminated by counterpropagating beams with $\sigma^+$ and $\sigma^-$ polarizations [16]. Three additional complications arise in our case, however. First, the transition we are using in He* is of the form $J_{\rm g} = 1 \leftrightarrow J_{\rm e} = 2$ , therefore transient optical pumping effects may be very important. This is especially true if the field gradient is increasing rapidly. Second, it is well-known that optical pumping effects lead to friction mechanisms going beyond the above Doppler cooling model. In the case of He*, where the recoil and Doppler limits are not widely separated this is a difficult theoretical problem for which no analytic results are available. Since previous experiments [17] show that the temperatures achieved in optical molasses are not sub-Doppler for He*, we will not take into account these mechanisms. Thirdly, we use DBR diode lasers whose linewidth is of order 3–5 MHz (measured by recording a beat note between two independent lasers) which is somewhat larger than the natural linewidth of the $2^3{\rm S}_1 - 2^3{\rm P}_2$ transition (1.6 MHz). However, a numerical model indicates that,

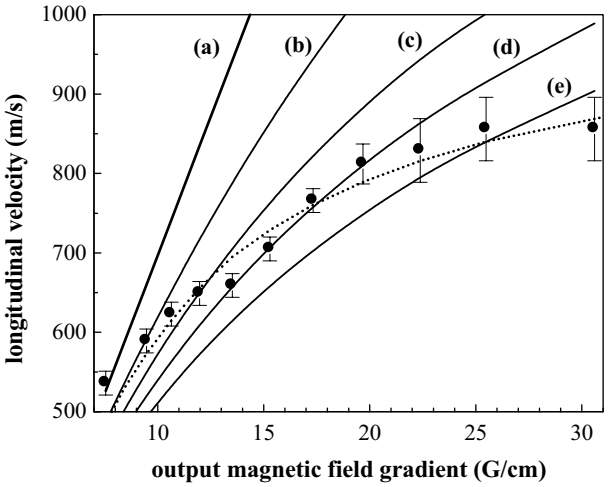


**Fig. 12.** Study of the focal length. The circles in this plot correspond to measured values of the magnetic field gradient and longitudinal velocity that lead to a *fixed* focal length $f = 46$ cm. The solid lines show the numerical solutions of equation (1), for different values of the damping coefficient $\gamma$: (a) $\gamma = \infty$ (no lag, expression (2)), (b) $\gamma = (9\ \mu\text{s})^{-1}$, (c) $\gamma = (17\ \mu\text{s})^{-1}$, (d) $\gamma = (23\ \mu\text{s})^{-1}$, (e) $\gamma = (29\ \mu\text{s})^{-1}$. The dotted line is a fit taking into account the tilt angle $\theta$ between the laser beams and the plane orthogonal to the atomic beam axis, which introduces a velocity-dependent $\gamma$; the parameter value for this fit is $\theta = 5$ mrad. The measured gradient profile was used in the calculation.

for our parameters, taking into account the laser linewidth hardly modifies the friction coefficient as calculated by equation (7). With these caveats we can estimate the value of the damping coefficient $\gamma$, for $I/I_0 = 5$ and $\Delta = -2\Gamma$ to be about $(17\ \mu\text{s})^{-1}$. However this value must be considered uncertain to within at least a factor of two. In addition, we do not know precisely the value of $\Delta$, which is obtained by slightly tilting the funnel beams as described in Section 3.

To find the form of the function $F(t)$ we have measured the variation of the field gradient in the interaction region using a Hall probe (see Fig. 4). These results can be used to calculate the integral in equation (4) numerically. The solid curves in Figure 12 represent the predicted values for $v_z\,(b_\text{f})$ for the measured variation of $F(t)$ and for various values of the damping rate $\gamma$. We see that there appears to be some significant deviations from our model, assuming $\gamma$ constant. Indeed the observed behavior seems consistent with a $\gamma$ decreasing as the beam velocity (and the field gradient) increases. This evolution is understandable because, in the experiment, the laser beams are deliberately aligned at an angle $\theta$ with respect to the plane orthogonal to the atomic beam axis. This tilt produces a (red) detuning, which depends on the longitudinal velocity $v_z$. Thus the friction coefficient should also vary with velocity. The value of $\theta$ is not known accurately, but we can fit the experimental data using equation (7) to compute the damping rate with $\theta$ an adjustable parameter. The dotted line in Figure 12 shows such a fit with $\theta = 5$ mrad. The agreement is quite satisfactory.

The model of a damped harmonic oscillator whose position does not vary within the interaction region thus appears to be a useful model of the behavior of the atoms in the funnel. An important new result of the model is that the finite velocity damping time can affect the position of the focus. The effect is significant if the damping rate $\gamma$ is not large compared to $\beta$, the rate at which the magnetic field gradient increases during the interaction time.

## 6 Applications and prospectives

As we have mentioned, the funnel is capable of taking an arbitrary input phase space and, provided that it is within its capture range, mapping it onto a spot. This happens at a distance determined largely by the magnetic field gradient. One application of this technique is to use a time-varying transverse magnetic field to scan the atomic beam. In principle this can be done on a time scale of order $t_\text{int} = z_\text{int}/v_z$, about 100 $\mu$s in our experiment. We have demonstrated this modulation by adding transverse coils to displace the zero of the field gradient. We can easily displace a 600 m/s beam by at least $\pm 0.5$ cm, without any distortion of the beam profile.

A second possibility, as was also pointed out in reference [18], is to perform the analogous operation in the time domain on a 3D MOT. A large spatial distribution can be transiently compressed by ramping up the magnetic field and then switching off the lasers. Compared to other MOT compression schemes, this technique has the advantage that when the atoms reach a high density, no lasers are present and thus losses or repulsive effects [19] due to the presence of the lasers are absent. This is particularly useful for He* where it is known that large light dependent losses are present [12]. A large cloud such as was used in reference [13] could be compressed with little loss of atoms to a 1 mm size, by ramping up the field gradient to 20 G/cm in 100 ms – and interesting situation for studying collisions.

This work is funded by Région Ile de France. BW and WR are funded by grants from the EU. GL gratefully acknowledges financial support from Thomson-CSF and wish to thanks J.-P. Pocholle for stimulating discussions.

## References

1. K. Berggren, A. Bard, J. Wilbur, J. Gillaspy, A. Helg, J. McClelland, S. Rolston, W. Phillips, M. Prentiss, G. Whitesides, Science **269**, 1255 (1995).
2. S. Nowak, T. Pfau, J. Mlynek, Appl. Phys. B **63**, 203 (1996).
3. K. Johnson, M. Drndic, J. Thywissen, G. Zabow, R. Westervelt, M. Prentiss, Phys. Rev. Lett. **81**, 1137 (1998).
4. W. Rooijakkers, W. Hogervorst, W. Vassen, Opt. Commun. **123**, 321 (1996).
5. M. Joffe, W. Ketterle, A. Martin, D. Pritchard, JOSA B **10**, 2257 (1993).

6. M. Hoogerland, J. Driessen, E. Vredenbregt, H. Megens, M. Schuwer, H. Beijerinck, K. van Leeuwen, Appl. Phys. B **62**, 323 (1996).
7. E. Raab, M. Prentiss, A. Cable, S. Chu, D. Pritchard, Phys. Rev. Lett. **59**, 263 (1987).
8. J. Nellessen, J. Werner, W. Ertmer, Opt. Commun. **78**, 300 (1990).
9. E. Riis, D. Weiss, K. Moler, S. Chu, Phys. Rev. Lett. **64**, 1658 (1990).
10. T. Swanson, N. Silva, S. Mayer, J. Maki, D. McIntyre, J. Opt. Soc. B **13**, 1833 (1996).
11. A. Steane, M Chowdhury, C. Foot, J. Opt. Soc. B **9**, 2142 (1992).
12. F. Bardou, O. Emile, J.-M. Courty, C. Westbrook, A. Aspect, Europhys. Lett. **20**, 681 (1992).
13. W. Rooijakkers, W. Hogervorst, W. Vassen, Opt. Commun. **135**, 149 (1997).
14. H. Mastwijk, M. van Rijnbach, J. Thomsen, P. van der Straten, A. Niehaus, Eur. J. Phys. D (submitted, 1998).
15. G. Labeyrie, Ph.D. thesis, University of Paris-sud, 1998.
16. P. Lett, W. Phillips, S. Rolston, C. Tanner, R. Watts, C. Westbrook, J. Opt. Soc. B **6**, 2084 (1988).
17. F. Bardou, Ph.D. thesis, University of Paris XI, 1995.
18. V. Balykin, JETP Lett. **66**, 349 (1997).
19. D. Sesko, T. Walker, C. Wieman, J. Opt. Soc. B **8**, 946 (1991).